Ionics (2022) 28:3935–3944
https://doi.org/10.1007/s11581-022-04631-2

ORIGINAL PAPER

# Three-dimensional self-supporting $Ni_2P$-$Ni_{12}P_5$/NF heterostructure as an efficient electrocatalyst to enhance hydrogen evolution reaction

Yanxia Wu[1] · Xiangping Chen[1] · Lirong Su[1] · Qingtao Wang[1] · Shufang Ren[2]

Received: 2 March 2022 / Revised: 8 May 2022 / Accepted: 29 May 2022 / Published online: 15 June 2022


## Abstract

Increasing active sites by constructing a heterostructure is a very effective method to improve the electrocatalytic performance. In this work, we synthesized a three-dimensional self-supporting $Ni_2P$-$Ni_{12}P_5$/NF heterostructure supported on nickel foams by hydrothermal reaction and low-temperature phosphorization, used as an efficient hydrogen evolution reaction (HER) electrocatalyst. The structure, composition, morphology, and HER performance of the catalyst were characterized by XRD, XPS, SEM, TEM, and electrochemical workstation. The experimental results show that the $Ni_2P$-$Ni_{12}P_5$/NF heterostructure demonstrates better HER catalytic activity in 0.5 M $H_2SO_4$, only requiring an overpotential of 124 mV at 10 mA $cm^{-2}$ with a Tafel slope of 84.1 mV $dec^{-1}$ and displaying good long-term stability. The high activity and stability of the as-synthesized $Ni_2P$-$Ni_{12}P_5$/NF catalyst in HER are mainly due to the synergy between $Ni_2P$-$Ni_{12}P_5$ with a unique heterostructure and nickel foam conductive substrate with a three-dimensional porous structure, which is beneficial to increase the electrocatalytic active area and thus provide more active sites.

**Keywords** Nickel phosphide · Electrocatalyst · Heterostructure · Hydrogen evolution reaction · Electrolysis of water

## Introduction

With the rapid development of social economy and the continuous growth of the population, people's demand for energy is increasing [1, 2]. Long-term use of traditional fossil fuels will accelerate the energy crisis, climate change, and environmental pollution. Therefore, it is an irresistible trend to develop clean, efficient, and renewable alternative energy, such as wind energy, hydrogen energy, solar energy, and biomass energy [1–3]. However, much renewable energy cannot be effectively utilized because of their instability, intermittence, and regionality. As an energy carrier, hydrogen has the advantages of high energy density, non-toxicity, wide range of sources, environmentally friendliness, and so on, which is considered to be one of the most promising renewable clean energy alternatives to fossil fuels [4, 5]. The development of hydrogen production technology is of great practical significance to relieve energy crisis and environmental problems, and realize the sustainable development of energy. Electrochemical water splitting is recognized to be the most promising way to achieve sustainable energy development and zero emission in the current hydrogen production technologies [6, 7]. However, because of its slow reaction kinetics for HER, it is necessary to design and develop effective electrocatalysts that can reduce HER overpotential [8]. At present, noble metal platinum-based catalysts exhibit outstanding HER catalytic activity. Unfortunately, such catalysts have the disadvantages of limited earth reserves and high price, which limit their large-scale industrial applications [9]. Therefore, it is urgent to develop non-noble metal–based catalysts with abundant reserves, low cost, high efficiency, and stability, which is very important to realize the industrial application of hydrogen production by electrochemical water splitting.

At present, the most studied non-noble metal HER catalysts are transition metal compounds, such as sulfides [10], selenides [11, 12], and phosphides [13–16]. Especially,

✉ Yanxia Wu
wuyx2014@nwnu.edu.cn

✉ Qingtao Wang
wangqt@nwnu.edu.cn

[1] Key Laboratory of Eco-Functional Polymer Materials of the Ministry of Education, College of Chemistry and Chemical Engineering, Northwest Normal University, Lanzhou 730070, China

[2] Key Laboratory of Evidence Science Research and Application of Gansu Province, Gansu University of Political Science and Law, Lanzhou 730070, China

transition metal phosphides have been widely studied as HER catalysts in recent years because of their abundant reserves, low cost, good conductivity, and stable catalytic activity. But they show higher overpotential, slower charge transfer, and poorer conductivity compared with noble metal platinum-based catalysts. So, a variety of modification methods have been proposed, such as morphological controlling [17, 18], compounding [19, 20], and doping [21–26]. Sumboja et al. [18] synthesized the alveolar sac–like morphology of cobalt phosphide (Co-P I) and randomly shaped nanoparticles of cobalt phosphide (Co-P II). Compared with Co-P II, Co-P I displayed better catalytic activity in acidic and alkaline media, which was due to that its unique structure could increase the catalytic active area, contributing to enhance HER activity. Ge et al. [21] reported that well-crystallized molybdenum phosphide was dispersed on graphene carbon nanosheets co-doped with N and P (MoP/NPG). The results showed that the coupled interfaces and synergistic effect between MoP and graphene substrate could promote charge transfer kinetics and improve its catalytic activity. Gao et al. [27] revealed that rare-earth elemental Ce was doped into CoP to improve HER performance by modulating electronic structures and decreasing adsorption free energy of hydrogen. The above modification methods have significantly improved the HER performance of catalysts, but the insufficient active sites are still the key to affect catalytic activity. In recent years, constructing heterojunction by interface engineering has been recognized as an effective method to further improve the HER electrocatalytic performance of materials [28–31]. Boppella et al. [32] synthesized two-dimensional cobalt phosphide/nickel cobalt phosphide (CoP/NiCoP) heterojunction nanosheets supported by nitrogen-doped carbon. The collective effects of electronic structure engineering and strong interfacial coupling between CoP and NiCoP in heterojunction improved the reaction kinetics and catalytic performance of HER. Yan et al. [33] successfully prepared $Ni_2P$-$Ni_5P_4$ heterostructure nanosheet arrays by simply tuning the reaction temperatures. The abundant catalytic active sites, large surface areas, highly conductive support of carbon cloth substrates, and unique free-standing arrays could enhance kinetics and electrocatalytic performances for the HER, oxygen evolution reaction (OER) and overall water splitting.

These studies reveal that porous nickel phosphides have good conductivity and large surface area, which can provide abundant active sites and accelerate electron transportation and charges transfer [34, 35]. Constructing a heterostructure through different nickel phosphide phases can effectively increase electroactive sites, contributing to improve catalytic activity [33]. At the same time, the three-dimensional porous nickel foam substrate possesses large surface area, high structural porosity, and fast electron transport channels, which are beneficial for electron transport and mass transfer. Wang et al. [36] prepared a self-supported $Ni_5P_4$-$Ni_2P$ nanosheet (NS) array by directly phosphating nickel foam with phosphorus vapor, which showed better electrocatalytic activity and long-term persistence for HER in acidic medium. Herein, we constructed a self-supporting $Ni_2P$-$Ni_{12}P_5$/NF heterostructure catalyst supported on three-dimensional porous nickel foam substrate through hydrothermal reaction and low-temperature phosphorization. The synergy between the $Ni_2P$-$Ni_{12}P_5$ heterostructure and the three-dimensional porous nickel foam substrate effectively enhanced the HER electrocatalytic activity and stability of the catalyst.

## Experimental section

### Materials

Hydrochloric acid, acetone, ethanol, and urea were supplied by Sinopharm Chemical Reagent Co., Ltd. Red phosphorus and nickel nitrate hexahydrate were obtained from Shanghai Zhongqin Chemical Reagent Co., Ltd. Sodium hypophosphite monohydrate and ammonium fluoride were obtained from Yantai Shuangshuang Chemical Co., Ltd. Potassium hydroxide was purchased from Taicang Hushi Reagent Co., Ltd. Nickel chloride hexahydrate and sodium lauryl sulfate were produced by Shanghai Titan Technology Co., Ltd, and Shanghai Aladdin Biochemical Technology Co., Ltd., respectively. All chemicals utilized were of analytical grade and were used as supplied without any further purification.

### Material preparation

Nickel nitrate hexahydrate (2 mmol), ammonium fluoride (6 mmol), and urea (10 mmol) were added to 30 mL of deionized water, forming a green homogeneous mixture after ultrasonicating for 1 h. The above mixture and acid-washed nickel foams (NF) were introduced into a 50 mL high-pressure reactor and kept at 120 °C for 6 h in the oven. The obtained solid was washed with ethanol and deionized water, and then placed in a vacuum oven at 60 °C to completely dry to obtain a Ni(OH)F/NF precursor [37]. Ni(OH)F/NF was placed in a tube furnace and then heated to 450 °C for 2 h at a heating rate of 5 °C $min^{-1}$ in air atmosphere to obtain NiO/NF. The subsequent phosphorization was carried out in Ar atmosphere by gradually heating sodium hypophosphite monohydrate and NiO/NF to 350 °C at a heating rate of 3 °C $min^{-1}$ for 2 h. The product was naturally cooled to room temperature, washed with ethanol and deionized water alternately for several times, and dried in a vacuum oven at 60 °C to obtain the material $Ni_2P$-$Ni_{12}P_5$/NF. The preparation process of the $Ni_2P$-$Ni_{12}P_5$/NF is shown

in Fig. 1. The preparation process of $Ni_2P$ was given in the Supporting Information.

## Material characterizations

X-ray diffraction (XRD) tests were performed on a D/Max 2400 powder diffractometer to analyze crystal phases of the as-synthesized materials. Scanning electron microscopy (SEM) was conducted on JSM-6701F to characterize the morphology of the materials. Transmission electron microscopy (TEM) and energy-dispersive X-ray (EDX) spectrometry measurements were carried out on TF20 to characterize lattice fringes and chemical elements. X-ray photoelectron spectroscopy (XPS) characterization was performed on a PHI 5702 XPS instrument to analyze the chemical compositions and valence states of the materials.

## Electrochemical measurements

All the electrochemical measurements were conducted on a three-electrode electrochemical cell by an Autolab PGSTAT128N electrochemical workstation. $Ni_2P$-$Ni_{12}P_5$/NF and other samples as controls were used as the working electrode. Ag/AgCl and Hg/HgO were used as the reference electrodes in acidic and alkaline electrolytes, respectively. The graphite rod was used as counter electrode. Electrochemical tests were performed in 0.5 M $H_2SO_4$ and 1.0 M KOH electrolytes, respectively. The presented potentials in this work were all converted to reversible hydrogen electrode (RHE) via the equation: $E$ (RHE) = $E$ (Ag/AgCl) + 0.059 pH + 0.197 (in acidic electrolyte) and $E$ (RHE) = $E$ (Hg/HgO) + 0.059 pH + 0.098 (in alkaline electrolyte). All of the polarization curves were recorded using linear sweep voltammetry (LSV). Electrochemical impedance spectroscopy (EIS) measurements were performed at the corresponding open-circuit potential to the electrode. The frequency range was 50 kHz–0.01 Hz. The charge-transfer resistance ($R_{ct}$) was calculated by the diameter of the semicircular arc in the Nyquist plots. The double-layer capacitance ($C_{dl}$) values were determined by performing cyclic voltammetry (CV) measurements at different scanning rates of 30 ~ 150 mV $s^{-1}$ under a non-Faradaic potential range. The Faradaic efficiency (FE) was evaluated by comparing the theoretical value with the amount of $H_2$ obtained from the experiment based on the current density of 10 mA $cm^{-2}$. The amount of produced $H_2$ was recorded by the drainage method. The calculation formula is FE (%) = $(m \times n \times F)/(I \times t)$. $m$ and $n$ represent the number of hydrogen production (mol) and electrons transferred by a hydrogen molecule, respectively. $F$ represents Faraday's constant (96,485 C $mol^{-1}$). $I$ and $t$ represent current (A) and time (s), respectively.

## Results and discussion

XRD tests were used to identify the crystal structure of materials. Figure 2a shows the XRD patterns of the as-synthesized $Ni_2P$ and $Ni_2P$-$Ni_{12}P_5$. The diffraction peaks of

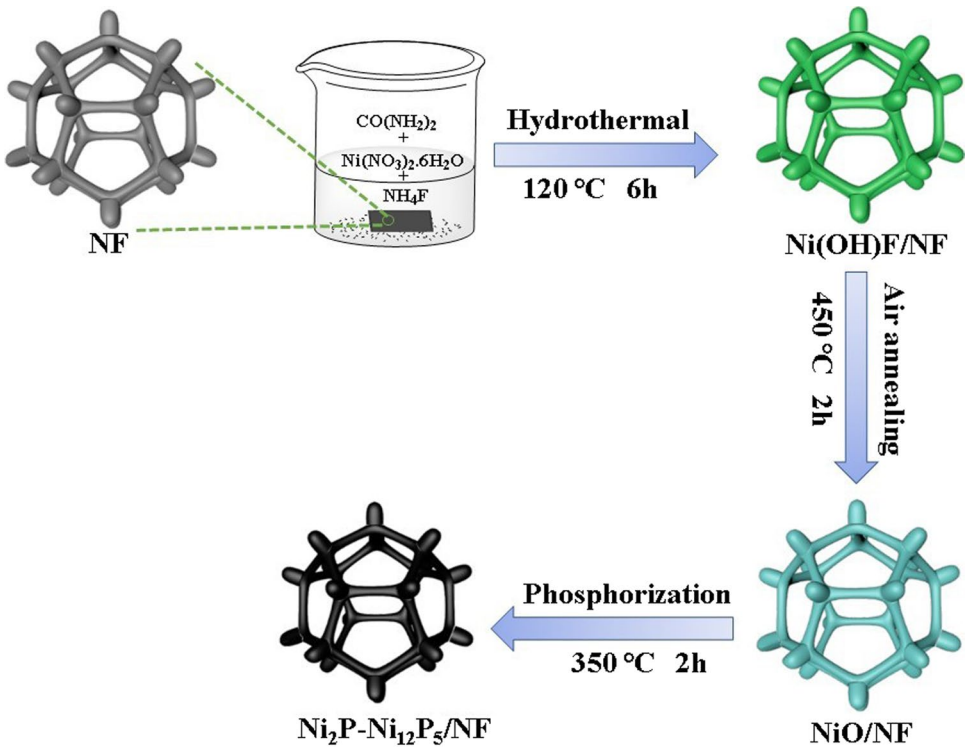


**Fig. 1** Preparation process of $Ni_2P$-$Ni_{12}P_5$/NF

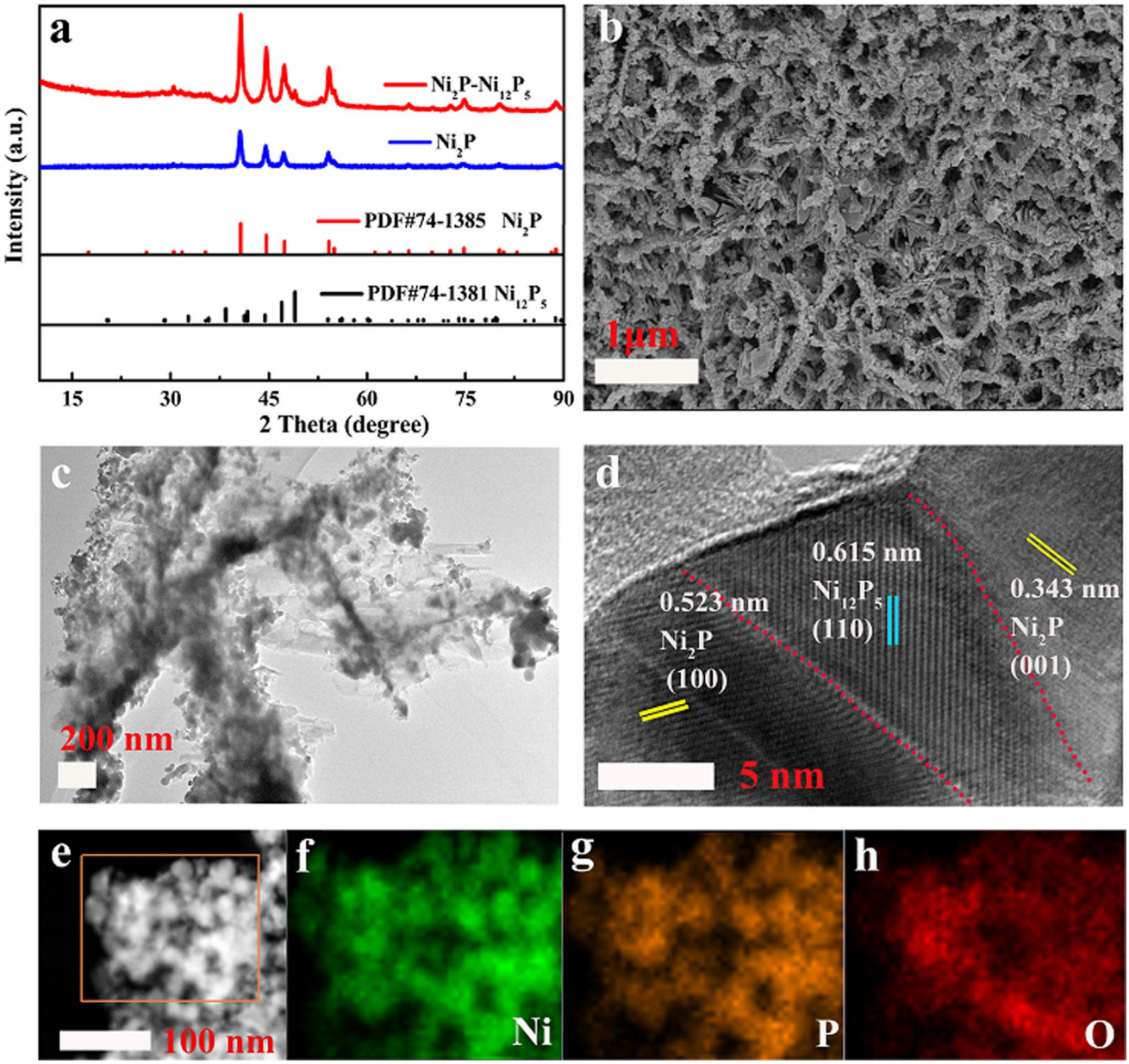


**Fig. 2** The characterizations of $Ni_2P$-$Ni_{12}P_5$/NF. **a** XRD patterns, **b** SEM image, **c** TEM image, **d** HRTEM image, **e–h** HAADF-STEM image and EDX elemental mappings

$Ni_2P$-$Ni_{12}P_5$ can be well indexed to $Ni_2P$ (PDF#74–1385) and $Ni_{12}P_5$ (PDF#74–1381). The peaks at 40.7, 44.6, 47.4, 54.3, and 55.1° are indexed to (111), (201), (210), (300), and (211) crystal planes of $Ni_2P$, respectively. The diffraction peaks appeared at 48.9, 46.9, and 38.4° are corresponding to (312), (240), and (112) crystal planes of $Ni_{12}P_5$, respectively. This indicates that two kinds of nickel phosphide were successfully prepared by hydrothermal reaction and the followed low-temperature phosphorization. The diffraction peaks of the pure $Ni_2P$ are also well indexed to $Ni_2P$ (PDF#74–1385). The XRD pattern of NiO was given in Fig. S1a (Supporting Information).

Figure 2b shows the SEM image of $Ni_2P$-$Ni_{12}P_5$/NF. It can be seen that $Ni_2P$-$Ni_{12}P_5$/NF is characterized with a three-dimensional porous structure composed of nanoparticles and nanosheets. As shown in Fig. S1b, the precursor NiO/NF covered on nickel foams with a sheet structure composed of nanoparticles. NiO/NF was phosphorized with $PH_3$ gas that was generated by in-situ thermal decomposition of sodium hypophosphite to form $Ni_2P$-$Ni_{12}P_5$/NF

with a three-dimensional porous structure of nanoparticles and nanosheets. This porous structure is capable not only of increasing catalytic active areas of the material, but also of contributing to improve HER performance. TEM image in Fig. 2c reveals that $Ni_2P$-$Ni_{12}P_5$ possesses a three-dimensional porous structure composed of nanoparticles and nanosheets, in agreement with the results of its SEM image (Fig. 2b). The high-resolution TEM was further performed to confirm the boundary of $Ni_2P$ and $Ni_{12}P_5$, as shown in Fig. 2d. We can see that the lattice fringes with distances of 0.523 and 0.343 nm correspond to (100) and (001) planes of $Ni_2P$ (PDF#74–1385), respectively, and the lattice fringe with distance of 0.615 nm corresponds to the (110) plane of $Ni_{12}P_5$ (PDF#74–1381), which are consistent with the XRD results. The boundary of $Ni_2P$ and $Ni_{12}P_5$ can be clearly observed, proving the successful preparation of the $Ni_2P$-$Ni_{12}P_5$ heterostructure. The element composition and distribution of the material were analyzed by the EDX attached to the TEM instrument, as shown in Fig. 2e–h. It demonstrates the existence of Ni, P, and O elements in the material. The oxygen element may be caused by the slight surface oxidation of the material exposed in air.

The surface chemical compositions and valence of the $Ni_2P$-$Ni_{12}P_5$ heterostructure were investigated by XPS. The XPS survey spectrum of $Ni_2P$-$Ni_{12}P_5$ shows the presence of C, O, Ni, and P elements in the sample (Fig. 3a), which is basically consistent with the results of EDX. Ni 2p and P 2p spectra of $Ni_2P$-$Ni_{12}P_5$ and $Ni_2P$ are shown in Fig. 3 b and c, respectively. In Fig. 3b, the two peaks of $Ni_2P$-$Ni_{12}P_5$ located at 870.5 and 853.1 eV correspond to the Ni $2p_{1/2}$ and Ni $2p_{3/2}$ of $Ni^{\delta+}$ species, and the two peaks appeared at 874.6 and 856.4 eV correspond to the Ni $2p_{1/2}$ and Ni $2p_{3/2}$ of $Ni^{x+}$ species, respectively. $Ni^{x+}$ species are assigned to nickel oxides due to the surface oxidation of the catalyst exposed in air, which is very common for the transition-metal phosphides[32, 35, 37]. Figure 3c shows that the two peaks of $Ni_2P$-$Ni_{12}P_5$ at the binding energies of 129.4 and 130.1 eV are ascribed to P $2p_{3/2}$ and P $2p_{1/2}$, respectively. The peak appeared at 133.4 eV may be P-O species due to the superficial oxidation of the catalyst exposed in air [38, 39]. Compared with $Ni_2P$, the peaks of Ni 2p in $Ni_2P$-$Ni_{12}P_5$ shift towards higher binding energy, while the peaks of P 2p shift towards lower binding energy, suggesting that the electron interaction between $Ni_2P$ and $Ni_{12}P_5$ leads to the charge redistribution at the coupling interface [32, 40, 41].

In order to evaluate the HER electrocatalytic performance of $Ni_2P$-$Ni_{12}P_5$/NF, the electrochemical tests were performed in 0.5 M $H_2SO_4$ and 1.0 M KOH using a standard three-electrode cell. Linear sweep voltammetry (LSV) plots in 0.5 M $H_2SO_4$ and 1.0 M KOH are shown in Figs. 4 and 5, respectively. The catalytic activities of NiO/NF, $Ni_2P$/NF, and Pt/C/NF were also investigated for comparison. All of the polarization curves of the samples above were collected without *iR* correction. As shown in Fig. 4a, the overpotential of $Ni_2P$-$Ni_{12}P_5$/NF is only 124 mV at a current density of 10 mA $cm^{-2}$ that is obviously much lower than those of $Ni_2P$/NF (308 mV) and NiO/NF (534 mV), exhibiting better HER catalytic activity. It may be due to the fact that heterostructure for $Ni_2P$-$Ni_{12}P_5$/NF could provide more catalytic active sites, promoting the HER electrocatalytic performance of the material.

The electrocatalytic kinetics and mechanism for HER were investigated by the Tafel slope obtained via fitting the linear regions of Tafel plot, which is an important parameter to evaluate catalytic activity of the catalysts. According to the HER mechanism for electrolysis of water, the theoretical values of Tafel slope for Volmer, Heyrovsky, and Tafel reaction as the rate-limiting step are 120, 40, and 30 mV $dec^{-1}$, respectively [42]. Figure 4b shows that the Tafel slope of $Ni_2P$-$Ni_{12}P_5$/NF is 84.1 mV $dec^{-1}$, indicating that the HER process undergoes Volmer-Heyrovsky mechanism [42, 43]. In addition, it is clearly observed that the Tafel slope of $Ni_2P$-$Ni_{12}P_5$/NF is much smaller than those of $Ni_2P$/NF (207.8 mV $dec^{-1}$) and NiO/NF (273.4 mV $dec^{-1}$). It demonstrates that the HER kinetics on the $Ni_2P$-$Ni_{12}P_5$/NF is faster than the contrast samples, displaying good HER activity. The HER activity of $Ni_2P$-$Ni_{12}P_5$/NF is better than that of most reported transition metal phosphide catalysts, as shown in Table S1.

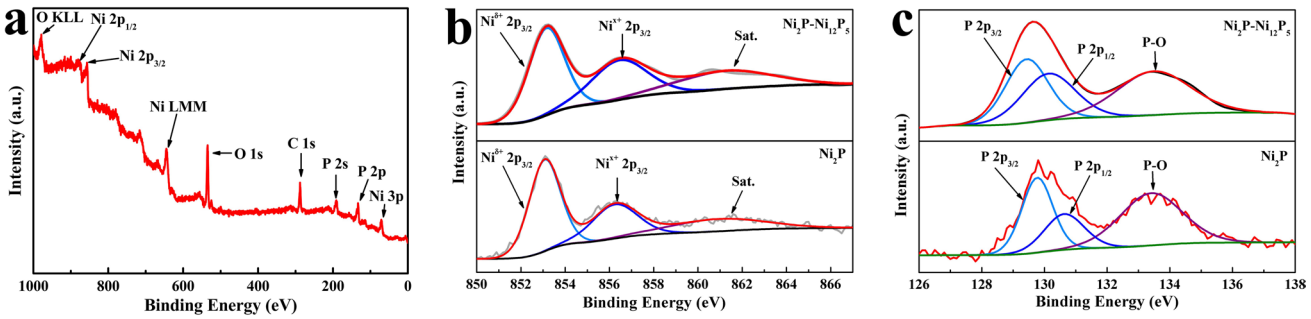


**Fig. 3** **a**XPS survey spectrum of $Ni_2P$-$Ni_{12}P_5$,**b** Ni 2p, and **c** P 2p spectra of $Ni_2P$-$Ni_{12}P_5$ and $Ni_2P$.

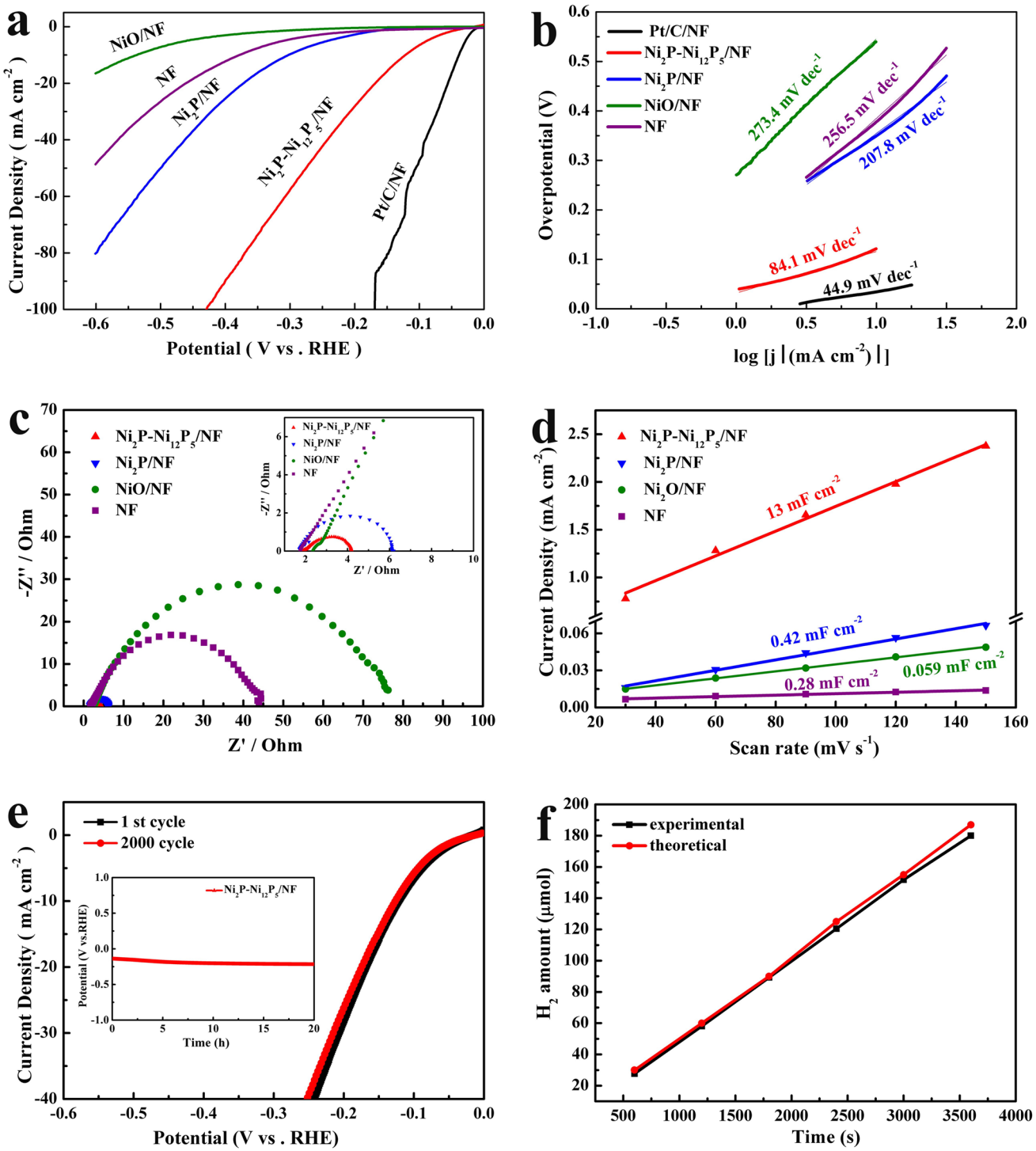


**Fig. 4** HER performance of different samples in 0.5 M $H_2SO_4$ solution. **a** LSV curves, **b** corresponding Tafel slopes, **c** Nyquist plots, the inset shows Nyquist plots magnified, **d** electrochemical double-layer capacitance, and **e** LSV curves of the $Ni_2P$-$Ni_{12}P_5$/NF before and after 2000 CV cycles; the inset shows the chronopotentiometric curve at a current density of 10 mA $cm^{-2}$ for 20 h. **f** Actual $H_2$ production versus theoretically calculated quantities for $Ni_2P$-$Ni_{12}P_5$/NF in 0.5 M $H_2SO_4$ under constant current density of 10 mA $cm^{-2}$

Electrochemical impedance spectroscopy (EIS) is an effective analytical technique to study the catalytic reaction kinetics at electrode/electrolyte interface, which can disclose the charge-transfer properties [7, 44]. The charge-transfer resistance ($R_{ct}$) was calculated through the diameter of the semicircular arc in the Nyquist plots, indicating the

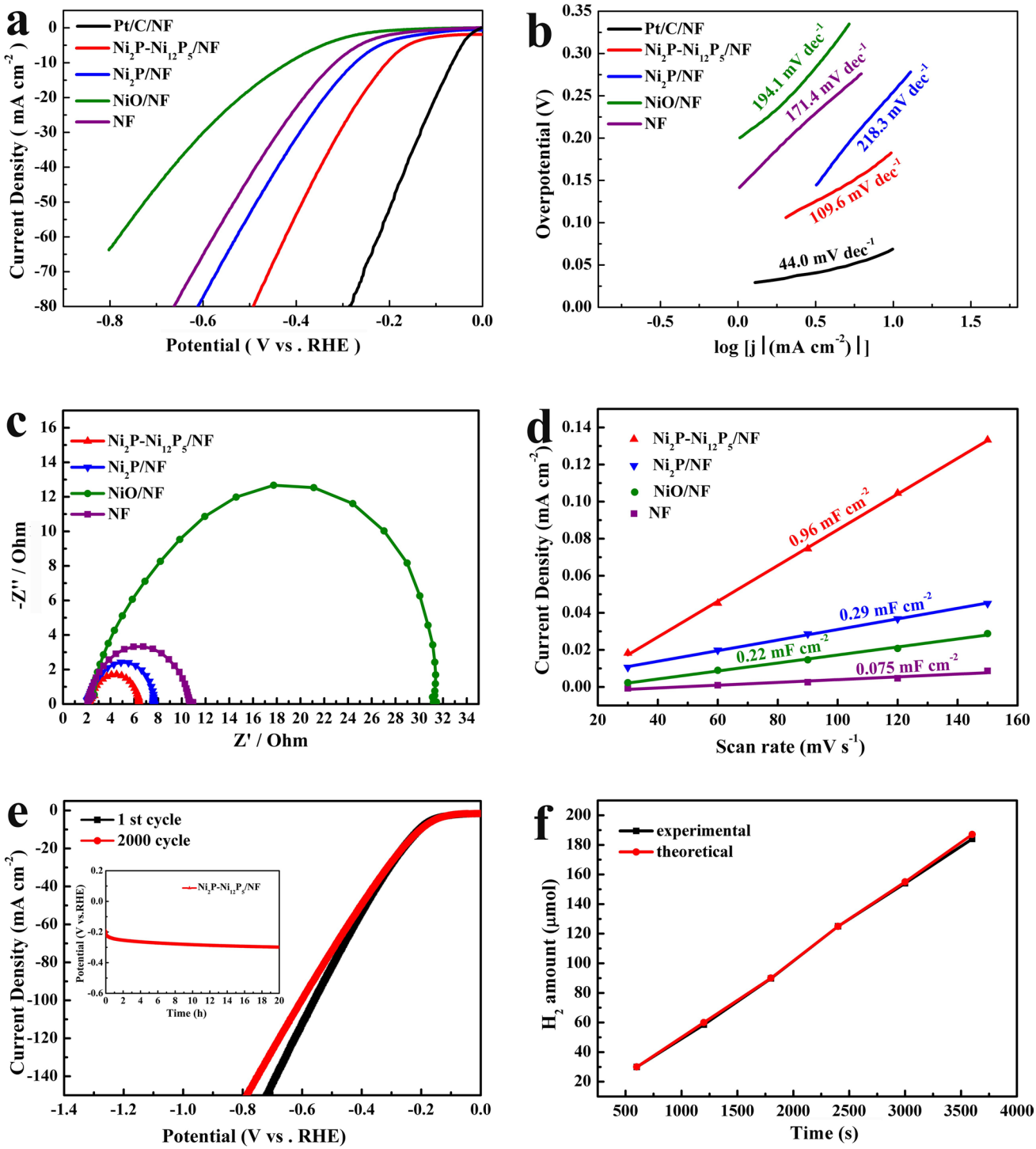


**Fig. 5** HER performance of different samples in 1.0 M KOH solution. **a** LSV curves, **b** corresponding Tafel slopes, **c** Nyquist plots, **d** electrochemical double-layer capacitance, **e** LSV curves of the $Ni_2P$-$Ni_{12}P_5$/NF before and after 2000 CV cycles; the inset shows the chronopotentiometric curve at a current of 10 mA $cm^{-2}$ for 20 h. **f** Actual $H_2$ production versus theoretically calculated quantities for $Ni_2P$-$Ni_{12}P_5$/NF in 1.0 M KOH under constant current density of 10 mA $cm^{-2}$

charge-transfer kinetics [13]. Figure 4c shows the Nyquist plots of the $Ni_2P$-$Ni_{12}P_5$/NF, $Ni_2P$/NF, and NiO/NF materials in the frequency range from 50 kHz to 0.01 Hz. It can be found that $Ni_2P$-$Ni_{12}P_5$/NF shows a much smaller semicircle than those of $Ni_2P$/NF and NiO/NF. The lower $R_{ct}$ of the $Ni_2P$-$Ni_{12}P_5$/NF demonstrates its higher intrinsic catalytic

activity and the faster charge-transfer rate at the electrode/electrolyte interface during the HER process [7, 45].

The electrochemically active surface area (ECSA) reveals the HER catalytic activity of catalysts, which is estimated by measuring the double-layer capacitance ($C_{dl}$) because of their positively proportional correlation [46–48]. The $C_{dl}$ values were obtained by performing cyclic voltammetry (CV) measurements at different scanning rates of 30–150 mV $s^{-1}$ under a non-Faradaic potential range in 0.5 M $H_2SO_4$ (Fig. S2). As shown in Fig. 4d, $Ni_2P$-$Ni_{12}P_5$/NF exhibits a $C_{dl}$ value of 13.9 mF $cm^{-2}$, which is much higher than those of $Ni_2P$/NF (0.42 mF $cm^{-2}$) and NiO/NF (0.059 mF $cm^{-2}$). The high $C_{dl}$ value of the $Ni_2P$-$Ni_{12}P_5$/NF heterostructure indicates the presence of abundant catalytic active sites, contributing to improve HER activity.

HER catalysts are required to possess not only good catalytic activity but also good stability. In practical applications, good stability means maintaining good catalytic activity for enough long time. So stability is an important index to evaluate the quality of the catalysts. The cycling stability of $Ni_2P$-$Ni_{12}P_5$/NF was examined by continuous CV with a potential scan from − 0.2 to − 0.8 V at a scan rate of 50 mV $s^{-1}$ for 2000 cycles. From the LSV curves in Fig. 4e, it can be seen that $Ni_2P$-$Ni_{12}P_5$/NF shows negligible degradation after 2000 CV cycles, demonstrating its superior cyclic stability in acidic media during HER process. In addition, the long-term stability of $Ni_2P$-$Ni_{12}P_5$/NF for HER was measured in 0.5 M $H_2SO_4$ using chronopotentiometry at controlled current density of 10 mA $cm^{-2}$ for 20 h. As displayed in the inset of Fig. 4e, $Ni_2P$-$Ni_{12}P_5$/NF exhibits a stable potential response for HER without significant degradation after continuous testing for 20 h, revealing preferable long-term stability.

Furthermore, the Faradaic efficiency (FE) of generated $H_2$ for the $Ni_2P$-$Ni_{12}P_5$/NF heterostructure was evaluated by comparing the theoretical value with the amount of $H_2$ obtained from the experiment based on the current density of 10 mA $cm^{-2}$, as shown in Fig. 4f. The amount of produced $H_2$ was recorded by the drainage method and the experimental value is very close to the theoretical value.

Figure 5 shows the HER tests of different catalysts in 1.0 M KOH solution. It can be seen from Fig. 5a and b that the overpotential of $Ni_2P$-$Ni_{12}P_5$/NF is 206 mV at a current density of 10 mA $cm^{-2}$ and Tafel slope is 109.6 mV $dec^{-1}$, which are obviously lower than those of $Ni_2P$/NF (275 mV, 218.3 mV $dec^{-1}$) and NiO/NF (428 mV, 194.1 mV $dec^{-1}$), displaying better HER catalytic activity in alkaline medium. As shown in Fig. 5c, the $R_{ct}$ value of $Ni_2P$-$Ni_{12}P_5$/NF is much lower than those of $Ni_2P$/NF and NiO/NF, exhibiting its faster charge-transfer rate for HER in alkaline medium. The $C_{dl}$ values were obtained by CV tests at different scanning rates of 30–150 mV $s^{-1}$ in 1.0 M KOH solution (Fig. S3). As displayed in Fig. 5d, the $Ni_2P$-$Ni_{12}P_5$/NF shows a higher $C_{dl}$ value (0.96 mF $cm^{-2}$) than $Ni_2P$/NF (0.29 mF $cm^{-2}$) and NiO/NF (0.22 mF $cm^{-2}$), indicating its good HER activity. The stability of the $Ni_2P$-$Ni_{12}P_5$/NF catalyst for HER was also measured in 1.0 M KOH. Figure 5e shows that the polarization curve obtained after 2000 cycles of the CV test displays slight degradation. The chronopotentiometry curve from the inset in Fig. 5e reveals that $Ni_2P$-$Ni_{12}P_5$/NF maintains good activity after continuous testing for 20 h, displaying better long-term durability in alkaline medium. Figure 5f shows that the FE of produced $H_2$ for $Ni_2P$-$Ni_{12}P_5$/NF in 1.0 M KOH at current density of 10 mA $cm^{-2}$ is almost 100%.

Based on the above electrochemical analysis results, the as-synthesized $Ni_2P$-$Ni_{12}P_5$/NF heterostructure displays better HER electrocatalytic activity and outstanding stability, especially in acidic medium, which can be ascribed to its unique structure and composition. First, the unique heterostructure formed between $Ni_2P$ and $Ni_{12}P_5$ leads to a strong electronic interaction at the interface, thereby modulating the electronic structure [49, 50], optimizing the adsorption of hydrogen, increasing the number of active sites, and accelerating the charge transfer rate [33, 51, 52]. It is beneficial to improve HER electrocatalytic activity of the catalyst. Second, the three-dimensional porous nickel foam substrate with large surface area is beneficial for not only generating highly exposed catalytically active sites, but also providing many transport channels for accelerating interfacial charge transfer. In addition, the synergistic effect between the $Ni_2P$-$Ni_{12}P_5$ heterostructure and nickel foam substrate effectively improves the HER electrocatalytic activity and stability of the as-synthesized catalyst.

## Conclusions

In summary, to design an effective HER electrocatalyst, a three-dimensional porous self-supporting $Ni_2P$-$Ni_{12}P_5$/NF heterostructure was successfully synthesized by hydrothermal reaction and low-temperature phosphorization. The as-synthesized $Ni_2P$-$Ni_{12}P_5$/NF catalyst exhibits better catalytic activity and stability for HER, especially in acidic medium. It only requires the low overpotential of 124 mV to drive a current density of 10 mA $cm^{-2}$ with a Tafel slope of 84.1 mV $dec^{-1}$ in 0.5 M $H_2SO_4$, showing better electrocatalytic performance than $Ni_2P$/NF. The synergistic effect between $Ni_2P$-$Ni_{12}P_5$ with a unique heterostructure and nickel foam substrate with three-dimensional porous structure contributes to the improvement of HER catalytic activity and the stability of the catalyst.

**Supplementary information** The online version contains supplementary material available at https://doi.org/10.1007/s11581-022-04631-2.

**Funding** This work was supported by the National Natural Science Foundation of China (Grant No. 21865032) and the Outstanding Graduate Student "the Star of Innovation" Project of Gansu Province (No. 2021CXZX-285).

## Declarations

**Competing interests** The authors declare no competing interests.

## References

1. Mahmood N, Yao Y, Zhang JW, Pan L, Zhang X, Zou JJ (2018) Electrocatalysts for hydrogen evolution in alkaline electrolytes: mechanisms, challenges, and prospective solutions. Advanced Science 5:1700464
2. Yao Z, Zhang M, Wu H, Yang L, Li R, Wang P (2015) Donor/acceptor indenoperylene dye for highly efficient organic dye-sensitized solar cells. J Am Chem Soc 137:3799–3802
3. Yao ZY, Zhang M, Li RZ, Yang L, Qiao Y, Wang P (2015) A metal-free N-annulated thienocyclopentaperylene dye: power conversion efficiency of 12% for dye-sensitized solar cells. Angew Chem Int Ed 54:5994–5998
4. Zhang JY, Wang H, Tian Y, Yan Y, Xue Q, He T, Liu HF, Yu C, Wang CD, Chen Y, Xia BY (2018) Anodic hydrazine oxidation assists energy-efficient hydrogen evolution over a bifunctional cobalt perselenide nanosheet electrode. Angew Chem Int Ed 57:7649–7653
5. Wang XG, Kolen'ko YV, Liu LF (2015) Direct solvothermal phosphorization of nickel foam to fabricate integrated $Ni_2P$-nanorods/Ni electrodes for efficient electrocatalytic hydrogen evolution. Chem Commun 51:6738–6741
6. Liu X, Ni K, Wen B, Guo R, Niu C, Meng J, Li Q, Wu P, Zhu Y, Wu X, Mai L (2019) Deep reconstruction of nickel-based precatalysts for water oxidation catalysis. ACS Energy Lett 4:2585–2592
7. Pei Y, Ge Y, Chu H, Smith W, Dong P, Ajayan PM, Ye M, Shen J (2019) Controlled synthesis of 3D porous structured cobalt-iron based nanosheets by electrodeposition as asymmetric electrodes for ultra-efficient water splitting. Appl Catal B 244:583–593
8. Feng JX, Xu H, Dong YT, Lu XF, Tong YX, Li GR (2017) Efficient hydrogen evolution electrocatalysis using cobalt nanotubes decorated with titanium dioxide nanodots. Angew Chem Int Ed 56:2960–2964
9. Ma M, Zheng Z, Song Z, Zhang X, Han X, Chen H, Xie Z, Kuang Q, Zheng L (2020) In situ construction and post-electrolysis structural study of porous $Ni_2P$@C nanosheet arrays for efficient water splitting. Inorganic Chem Front 7:2960–2968
10. Huang ZF, Song J, Li K, Tahir M, Wang YT, Pan L, Wang L, Zhang X, Zou JJ (2016) Hollow cobalt-based bimetallic sulfide polyhedra for efficient all-pH-value electrochemical and photocatalytic hydrogen evolution. J Am Chem Soc 138:1359–1365
11. Jing F, Lv Q, Wang Q, Chi K, Xu Z, Wang X, Wang S (2019) Self-supported 3D porous N-doped nickel selenide electrode for hydrogen evolution reaction over a wide range of pH. Electrochim Acta 304:202–209
12. Zhai L, Benedict Lo TW, Xu ZL, Potter J, Mo J, Guo X, Tang CC, Edman Tsang SC, Lau SP (2020) In situ phase transformation on nickel-based selenides for enhanced hydrogen evolution reaction in alkaline medium. ACS Energy Lett 5:2483–2491
13. Sun Y, Xu K, Zhao Z, Li X, Chen G, Li C (2020) Strongly coupled dual zerovalent nonmetal doped nickel phosphide nanoparticles/N, B-graphene hybrid for pH-universal hydrogen evolution catalysis. Appl Catal B 278:119284
14. Liang K, Pakhira S, Yang Z, Nijamudheen A, Ju L, Wang M, Aguirre-Velez CI, Sterbinsky GE, Du Y, Feng Z, Mendoza-Cortes JL, Yang Y (2018) S-doped MoP nanoporous layer toward high-efficiency hydrogen evolution in pH-universal electrolyte. ACS Catal 9:651–659
15. Liu T, Ma X, Liu D, Hao S, Du G, Ma Y, Asiri AM, Sun X, Chen L (2016) Mn doping of CoP nanosheets array: an efficient electrocatalyst for hydrogen evolution reaction with enhanced activity at all pH values. ACS Catal 7:98–102
16. Shi Y, Xu Y, Zhuo S, Zhang J, Zhang B (2015) $Ni_2P$ nanosheets/Ni foam composite electrode for long-lived and pH-tolerable electrochemical hydrogen generation. ACS Appl Mater Interfaces 7:2376–2384
17. Su L, Cui X, He T, Zeng L, Tian H, Song Y, Qi K, Xia BY (2019) Surface reconstruction of cobalt phosphide nanosheets by electrochemical activation for enhanced hydrogen evolution in alkaline solution. Chem Sci 10:2019–2024
18. Sumboja A, An T, Goh HY, Lubke M, Howard DP, Xu Y, Handoko AD, Zong Y, Liu Z (2018) One-step facile synthesis of cobalt phosphides for hydrogen evolution reaction catalysts in acidic and alkaline medium. ACS Appl Mater Interfaces 10:15673–15680
19. Wang X, Tong R, Wang Y, Tao H, Zhang Z, Wang H (2016) Surface roughening of nickel cobalt phosphide nanowire arrays/Ni Foam for enhanced hydrogen evolution activity. ACS Appl Mater Interfaces 8:34270–34279
20. Zhang Z, Shi X, Yang X (2016) Synthesis of core-shell NiSe/C nanospheres as anodes for lithium and sodium storage. Electrochim Acta 208:238–243
21. Ge R, Huo J, Liao T, Liu Y, Zhu M, Li Y, Zhang J, Li W (2020) Hierarchical molybdenum phosphide coupled with carbon as a whole pH-range electrocatalyst for hydrogen evolution reaction. Appl Catal B 260:118196
22. Liu T, Li P, Yao N, Cheng G, Chen S, Luo W, Yin Y (2019) CoP-doped MOF-based electrocatalyst for pH-universal hydrogen evolution reaction. Angew Chem Int Ed 58:4679–4684
23. Guan C, Xiao W, Wu H, Liu X, Zang W, Zhang H, Ding J, Feng YP, Pennycook SJ, Wang J (2018) Hollow Mo-doped CoP nanoarrays for efficient overall water splitting. Nano Energy 48:73–80
24. Tang C, Zhang R, Lu W, He L, Jiang X, Asiri AM, Sun X (2017) Fe-doped CoP nanoarray: a monolithic multifunctional catalyst for highly efficient hydrogen generation. Adv Mater 29:1602441
25. Wang H, Wang Y, Zhang J, Liu X, Tao S (2021) Electronic structure engineering through Fe-doping CoP enables hydrogen evolution coupled with electro-fenton. Nano Energy 84:105943
26. Wen S, Chen G, Chen W, Li M, Ouyang B, Wang X, Chen D, Gong T, Zhang X, Huang J, Ostrikov K (2021) Nb-doped layered FeNi phosphide nanosheets for highly efficient overall water splitting under high current densities. J Mater Chem A 9:9918–9926
27. Gao W, Yan M, Cheung H-Y, Xia Z, Zhou X, Qin Y, Wong C-Y, Ho JC, Chang C-R, Qu Y (2017) Modulating electronic structure of CoP electrocatalysts towards enhanced hydrogen evolution by Ce chemical doping in both acidic and basic media. Nano Energy 38:290–296
28. Guo Y, Park T, Yi JW, Henzie J, Kim J, Wang Z, Jiang B, Bando Y, Sugahara Y, Tang J, Yamauchi Y (2019) Nanoarchitectonics for transition-metal-sulfide-based electrocatalysts for water splitting. Adv Mater 31:1807134
29. Xiao X, Huang D, Fu Y, Wen M, Jiang X, Lv X, Li M, Gao L, Liu S, Wang M, Zhao C, Shen Y (2018) Engineering NiS/$Ni_2P$ heterostructures for efficient electrocatalytic water splitting. ACS Appl Mater Interfaces 10:4689–4696
30. Zeng L, Sun K, Wang X, Liu Y, Pan Y, Liu Z, Cao D, Song Y, Liu S, Liu C (2018) Three-dimensional-networked $Ni_2P/Ni_3S_2$ heteronanoflake arrays for highly enhanced electrochemical overall-water-splitting activity. Nano Energy 51:26–36

31. Wang Z, Wang S, Ma L, Guo Y, Sun J, Zhang N, Jiang R (2021) Water-induced formation of $Ni_2P$-$Ni_{12}P_5$ interfaces with superior electrocatalytic activity toward hydrogen Evolution Reaction. Small 17:2006770
32. Boppella R, Tan J, Yang W, Moon J (2018) Homologous CoP/NiCoP heterostructure on N-doped carbon for highly efficient and pH-universal hydrogen evolution electrocatalysis. Adv Func Mater 29:1807976
33. Yan Y, Lin J, Bao K, Xu T, Qi J, Cao J, Zhong Z, Fei W, Feng J (2019) Free-standing porous $Ni_2P$-$Ni_5P_4$ heterostructured arrays for efficient electrocatalytic water splitting. J Colloid Interface Sci 552:332–336
34. Yu X, Yu ZY, Zhang XL, Zheng YR, Duan Y, Gao Q, Wu R, Sun B, Gao MR, Wang G, Yu SH (2019) "Superaerophobic" nickel phosphide nanoarray catalyst for efficient hydrogen evolution at ultrahigh current densities. J Am Chem Soc 141:7537–7543
35. Tang C, Zhang R, Lu W, Wang Z, Liu D, Hao S, Du G, Asiri AM, Sun X (2017) Energy-saving electrolytic hydrogen generation: $Ni_2P$ nanoarray as a high-performance non-noble-metal electrocatalyst. Angew Chem Int Ed 56:842–846
36. Wang X, Kolen'ko YV, Bao XQ, Kovnir K, Liu L (2015) One-step synthesis of self-supported nickel phosphide nanosheet array cathodes for efficient electrocatalytic hydrogen generation. Angew Chem Int Ed 54:8188–8192
37. Wang C, Yang H, Zhang Y, Wang Q (2019) NiFe alloy nanoparticles with hcp crystal structure stimulate superior oxygen evolution reaction electrocatalytic activity. Angew Chem Int Ed 58:6099–6103
38. Men Y, Li P, Zhou J, Cheng G, Chen S, Luo W (2019) Tailoring the electronic structure of $Co_2P$ by N doping for boosting hydrogen evolution reaction at all pH values. ACS Catal 9:3744–3752
39. Gu Y, Wu A, Jiao Y, Zheng H, Wang X, Xie Y, Wang L, Tian C, Fu H (2021) Two-dimensional porous molybdenum phosphide/nitride heterojunction nanosheets for pH-universal hydrogen evolution reaction. Angew Chem Int Ed 60:6673–6681
40. Li D, Zhou C, Yang R, Xing Y, Xu S, Jiang D, Tian D, Shi W (2021) Interfacial engineering of the $Co_xP$-$Fe_2P$ heterostructure for efficient and robust electrochemical overall water splitting. ACS Sustain Chem Eng 9:7737–7748
41. Liu C, Gong T, Zhang J, Zheng X, Mao J, Liu H, Li Y, Hao Q (2020) Engineering $Ni_2P$-$NiSe_2$ heterostructure interface for highly efficient alkaline hydrogen evolution. Appl Catal B 262:118245
42. Li Y, Wang H, Xie L, Liang Y, Hong G, Dai H (2011) $MoS_2$ nanoparticles grown on graphene: an advanced catalyst for the hydrogen evolution reaction. J Am Chem Soc 133:7296–7299
43. Wang L, Wu H, Xi S, Chua ST, Wang F, Pennycook SJ, Yu ZG, Du Y, Xue J (2019) Nitrogen-doped cobalt phosphide for enhanced hydrogen evolution activity. ACS Appl Mater Interfaces 11:17359–17367
44. Huang Z, Chen Z, Chen Z, Lv C, Humphrey MG, Zhang C (2014) Cobalt phosphide nanorods as an efficient electrocatalyst for the hydrogen evolution reaction. Nano Energy 9:373–382
45. Zhang X, Yu X, Zhang L, Zhou F, Liang Y, Wang R (2018) Molybdenum phosphide/carbon nanotube hybrids as pH-universal electrocatalysts for hydrogen evolution reaction. Adv Func Mater 28:1706523
46. Pan Y, Sun K, Liu S, Cao X, Wu K, Cheong WC, Chen Z, Wang Y, Li Y, Liu Y, Wang D, Peng Q, Chen C, Li Y (2018) Core-shell ZIF-8@ZIF-67-derived CoP nanoparticle-embedded N-doped carbon nanotube hollow polyhedron for efficient overall water splitting. J Am Chem Soc 140:2610–2618
47. Xu Q, Gao W, Wang M, Yuan G, Ren X, Zhao R, Zhao S, Wang Q (2020) Electrodeposition of NiS/$Ni_2P$ nanoparticles embedded in amorphous $Ni(OH)_2$ nanosheets as an efficient and durable dual-functional electrocatalyst for overall water splitting. Int J Hydrogen Energy 45:2546–2556
48. Huang M, Ge K, Dong G, Zhou Z, Zeng Y (2019) 3-Dimensional flower-like clusters of CoNiP nanofoils in-situ grown on randomly-dispersed rGO-Nanosheets with superior electrocatalysis for hydrogen evolution reactions. Int J Hydrogen Energy 44:13195–13204
49. Liang LL, Song G, Liu Z, Chen JP, Xie LJ, Jia H, Kong QQ, Sun GH, Chen CM (2020) Constructing $Ni_{12}P_5$/$Ni_2P$ heterostructures to boost interfacial polarization for enhanced microwave absorption performance. ACS Appl Mater Interfaces 12:52208–52220
50. Tian FY, Hou D, Zhang WM, Qiao XQ, Li DS (2017) Synthesis of a $Ni_2P$/$Ni_{12}P_5$ bi-phase nanocomposite for the efficient catalytic reduction of 4-nitrophenol based on the unique n-n heterojunction effects. Dalton Trans 46:14107–14113
51. Wang Y, Wang B, Chu W, Kong Y, Wu Q, Liu Z (2020) Engineering NiCoP/$Mo_xC$ heterojunction for highly efficient hydrogen evolution reaction in alkaline and acid solution. Int J Hydrogen Energy 45:28774–28782
52. Chen Z, Liu X, Xin P, Wang H, Wu Y, Gao C, He Q, Jiang Y, Hu Z, Huang S (2021) Interface engineering of NiS@$MoS_2$ core-shell microspheres as an efficient catalyst for hydrogen evolution reaction in both acidic and alkaline medium. J Alloy Compd 853:157352